

A Real-Time Bridge Pier Scouring Monitoring System Based on Hall-Effect Sensors

Chen-Chia Chen, Ssu-Ying Chen, Wen-Ching Chen, Gang-Neng Sung, Jin-Ju Chue, Chih-Ting Kuo,
Yi-Jie Hsieh, Chih-Chyau Yang, Chien-Ming Wu, and Chun-Ming Huang
Applied Research Laboratories, National Chip Implementation Center,
7F, No. 26, Prosperity Rd. I, Science Park,
Hsinchu City, Taiwan.
Email: ccchen@cic.narl.org.tw

Abstract—Scour around bridge pier is the major cause of bridge failure such as collapse resulted in loss of life and property. Most of available bridge pier scour sensors and approaches are very expensive, which is a challenge for mass deployment of numerous bridges. Our proposed scour monitor system utilized low-cost commercial sensors, hall-effect sensors (unit price < \$1) that are capable of real-time measuring bridge pier scour with resolution of ca. 2.5 cm, and overall cost for single sensor node of my proposed work is at least 40% less expensive than existing work. After scour event, the typical output voltage difference of ~ 10 mV and the signal-to-noise ratio of ~ 10 were observed. After simple modified setup, the output voltage difference could be reached to ~300 mV. Moreover, the master-slave architecture of bridge pier scour monitoring system has scalability and flexibility for mass deployment. This technique has the potential for further widespread implementation in the field.

Keywords-bridge; piers; scour; senso; hall-effect

I. INTRODUCTION

In the past few decades, global warming has increased dramatically in rainfall intensity, duration, and frequency, which resulted in harsh floods in Taiwan. Nevertheless, most mountains in Taiwan are very steep with slope gradients, so rivers in Taiwan are usually short and steep. When typhoons come and bring intensive rainfall, resulted in serious floods, even disaster flow [1]. It usually causes tremendous damages and loss of life and property. According to 2012 annual report by directorate general of highways, MOTC, there are ~ 9699 bridges of highway in Taiwan area, total length ~ 502021.8 m. Some of the crossing river bridges face serious challenges of bridge foundation scouring problem during harsh floods and disaster flow. Bridges lose their piers due to excessive pier scour and high flow velocities, which is one of the major causes for partial bridge collapse [2].

For more than a hundred years, bridge pier scour has been extensively studied in the world. Many methodologies and instruments have employed to measure and monitor the local pier scour depth, such as sonar, radar, and Time-Domain Reflectometry (TDR), Fiber Bragg Grating (FBG) sensor [3]. The sonar and radar sensor provide contactless measurement of streambed scouring near bridge pier and abutments, and usually used to show the final status of streambed after a flood. One of disadvantages of the sonar and radar is that they have limit for measuring status of streambed in real time as rush water contained sands, even rocks during a flood. A method of TDR measures the reflections that results from a fast-rising step pulse travelling

through a measurement cable. The depth of soil-water interface is determined by counting the round trip travel time of the pulse. However, the major drawback of TDR is that accuracy of TDR is strongly depended on environment temperature and humidity. Moreover, monitoring scour depth by FBG is depended on number of FBG elements. However, the cost of monitoring of the scour depth by FBG technique is higher than that of existing methods [4]. The costs of Radar and TDR are expensive due to high-speed hardware requirement. For example, a commercial TDR (Campbell Scientific Inc., TDR100) was used to real-time monitor scour evolution [5], and its price is about \$250. For FBG, optical devices such as laser, photo detectors and the optical fibers are very expensive. In addition, most of the existing methods used for scour detection are expensive and complicated, which is a major challenge for mass deployment to a lot of bridge piers.

In this study, we develop and verify proposed real-time bridge pier scouring monitoring system which has a gateway and sensor nodes as master-slave configuration. Each sensor node has a hall-effect sensor module; overall cost for single sensor node is about ~\$100, the cost includes components and Printed Circuit Boards (PCB) manufacturing and assembly. Our proposed solution is 40% less expensive than existing work (TDR). Furthermore, we also developed a Bridge Surveillance program for remotely accessing raw sensor data. The experimental results show that our proposed monitoring system can monitor pier scour process in real-time.

We start with an overview of our proposed architecture and experimental setups in related work in Section II. Section III presents the results provided from our experiments. Finally, we conclude this paper in Section IV.

II. DEVELOPMENT OF REAL-TIME BRIDGE PIER SCOUR MONITORING SYSTEM

Architecture of bridge pier scouring monitoring system

The architecture of real-time bridge pier scour monitoring system is shown in Figure 1. The architecture is based on master-slave configuration. A master sends commands to slave for controlling sensor node and accessing sensor data. The host controller communicates with gateway through Power Over Ethernet (POE) and Ethernet switch. The host controller sends a command to the gateway. When the gateway receives command, the gateway converted Ethernet command to RS485 command. After converting command, the gateway broadcasts to sensor

nodes. Since the command packet contains unique sensor ID, only specific sensor node returned sensor data to the host controller. We adopt both accelerometer and hall-effect sensor modules in our sensor node. In order to reduce number of wires in this study, POE is utilized. Simply connected 48V battery (3 packs in series for 48V with individual 16V lithium iron phosphate battery) to the POE adaptor (Cerio, POE-PE03), and used an Ethernet cable to connect the POE adaptor to the gateway and sensor node in series.

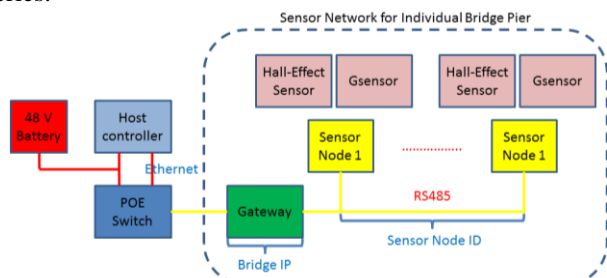


Figure 1: The architecture of real-time bridge pier scouring monitoring system

Gateway and Sensor nodes

The gateway is comprised of two stacked PCBs – a power module and a core module (see Figure 2). The top board is the power module, which operates as a DC-DC converter for creating 1.2~5V outputs from the 48V input. An Ethernet PHY (TI, DP83640) is used to receive and send Ethernet data, and also to send signals and power to sensor nodes through RS485 interface (ADI, ADM2682E). The core module is composed of a Cortex-R4 MCU (TI, RM48L952) and a FPGA (Xilinx, Spartan-6). Ethernet data and RS485 data are processed by the Cortex-R4 MCU and the FPGA, respectively. The FPGA mainly translates the sensor data from serial format to parallel format, between the FPGA and the Cortex-R4 MCU have three control signals (Int, Rdy, En) and 8-bit data signals. The FPGA receives the sensor data in 8-bit as a unit, after the FPGA collected 8-bit data, the FPGA will deposit to register, then send Int signal = 1 to the Cortex-R4 MCU, notify the Cortex-R4 MCU can receive sensor data. After the Cortex-R4 MCU receives 8-bit data, the Cortex-R4 MCU will set the Rdy signal to send a plus for the FPGA, followed by cycle until the FPGA En Signal = 0, on behalf of the sensor data has been transferred.



Figure 2: The photos of printed circuit boards of gateway (left) and sensor node (right).

The configuration of sensor node was similar to the gateway. The Cortex-R4 MCU is used to access sensor data through SPI (Serial Peripheral Interface) interface, and the FPGA is used to process RS485 data. The block diagram of the FPGA in sensor node is shown in figure 3.

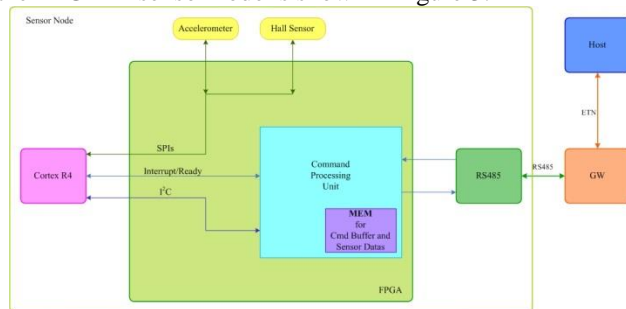


Figure 3: Block diagram of FPGA in sensor node

The FPGA parses receives commands, executes part of commands, and responses to the host. The Cortex-R4 MCU takes charge of collecting sensor data. Figure 4 describes processing sequence of the FPGA and the Cortex-R4 MCU. In Figure 4, the steps in blue are tasks of the FPGA, those in purple are memory related tasks, and those in red are tasks of the Cortex-R4 MCU. In the case that the host requests sensor data, the FPGA will receive a Read command. The FPGA then parses and decodes the command and is aware that cooperation with the Cortex-R4 MCU is necessary. The FPGA puts this command in memory and notifies the Cortex-R4 MCU with an interrupt. The Cortex-R4 MCU reads command from memory via I2C, collects sensor data and stores them in memory. After collection is done, the Cortex-R4 MCU notifies the FPGA with a General-Purpose Input/Output (GPIO) signal. Then the FPGA reads data from memory and generates response to the host.

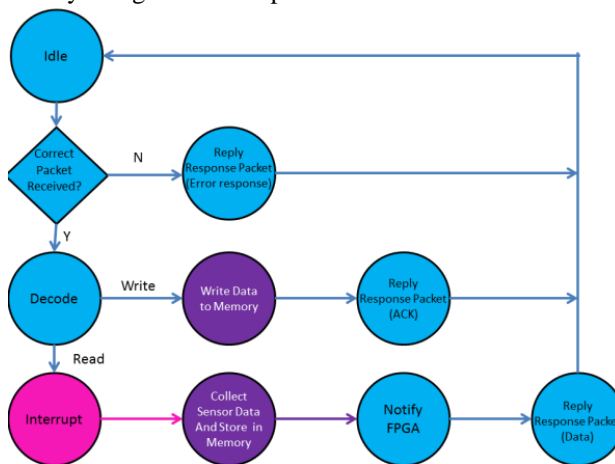


Figure 4: Processing sequence of FPGA and MCU

Accelerometer and hall-effect sensor modules

The core module of the sensor node which is connected to an accelerometer (ADI, ADXL345) and a hall-effect sensor (Allegromicro, A1301) which is used in this study are widely available online. But in this study, we only focus on the monitoring scour event by using the hall-effect sensors.

The output voltage of the hall-effect sensor is returned to an ADC (TI, ADS 1258) to digitize its analog signals, as shown in Figure 5. Digitizing output voltage of the hell-effect sensor sends back to the Cortex-R4 MCU via the SPI interface.



Figure 5: Top-view and bottom-view photos of the hall-effect sensor

Setup of the experimental tests

A Neodymium magnet with a diameter of 8 mm and thickness of 3 mm is fixed on thin metal strip with thickness of 0.3 mm, as shown in Figure 6. The hall-effect sensor and Neodymium magnet are aligned well, and are separated by a distance of 10 mm. Both types of sensor modules are installed along the pier model, as shown in Figure 7.

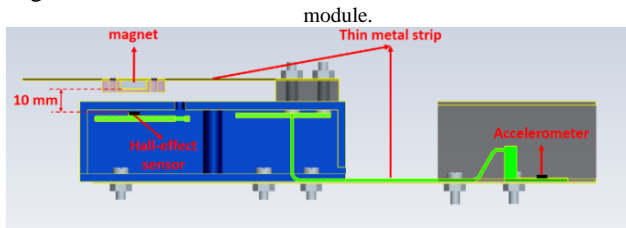


Figure 6: The drawing of house for accelerometer and hall-effect sensor module.



Figure 7: The photos of setup of real-time bridge pier scouring monitoring system.

The monitoring bridge scour erosion detection is carried out in a recirculating laboratory flume (length = 36m, width = 1 m, depth = 1.1 m) at Hydrotech Research Institute of National Taiwan University, Taiwan [6]. The layout of the flume and experimental setup are shown in Figure 8. A false test bed has a sediment recess (length = 2.8 m, width = 1 m, depth = 0.3 m) which is filled by nearly uniform sediment. A 15-cm-diameter hollow cylindrical pier made of plexiglass is located at the middle of the recess. An inlet valve and a

tailgate are used to regulate depths of flow and flow speed.

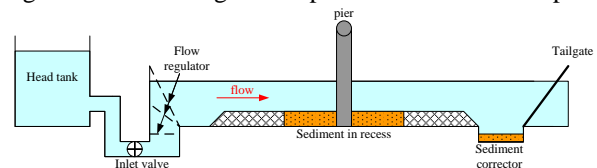


Figure 8: Partial layout of recirculating laboratory flume.

Gateway Initialization

The procedure including gateway initialization and sensor data access are shown in Figure 9. A Bridge Surveillance program is ran in the host controller, and it sends command (Request Packet) to specific gateway for making TCP connection through Ethernet. When the gateway receives ACK from the host controller and returned SYN/ACK, the TCP connection is made successes. The host controller sends a command to disconnect an active connection when the busy gateway does not return SYN/ACK. After making TCP connection, the gateway firstly initializes GPIO of the FPGA. Secondly, it converts Request Packet to serial data, and then it broadcasts serial data to sensor nodes. Until FPGA signal = 1, the FPGA receives sensor data from sensor node, and then the gateway sends the Response Packet to the host controller.

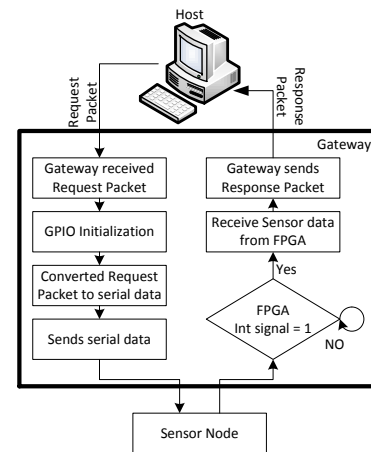


Figure 9: The flow chart of Gateway initialization

Figure 10 shows the Bridge Surveillance program with friendly graphical user interface, which automatically collects data from accelerometer and hall-effect sensor modules.

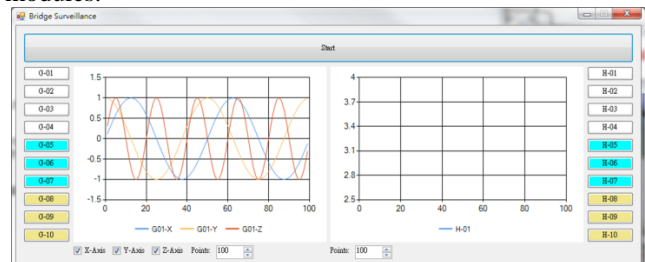


Figure 10: A Bridge Surveillance program with friendly graphical user interface (simulation data).

The host controller sends command every 20 ms, and the host controller will receive the Response Packet. The proposed software extracts the sensor data from payload of the Response Packet and then it displays them in real-time on charts (left: accelerometer, right: hall-effect sensor) of GUI as shown in Figure 10. Therefore, remote users can access raw data of each sensor nodes by WiFi communication, and they can analyze them in-situ. If pier scour status reaches critical condition of bridge collapse, the next version of the Bridge Surveillance program will alarm people away from the bridge.

III. RESULTS AND DISCUSSIONS

A simple method for calibrating the measuring gap between the hall-effect sensor and the magnet will be shown. A permanent magnet is moved away from the hall-effect sensor, and the dependence between corresponding output voltage of the hall-effect sensor and the distance between the magnet and the hall-effect sensor is shown in Figure 11. The output voltage of the hall-effect sensor as a function of the distance is nonlinear, but can be expressed by the following equation,

$$y = 7.513 - 1.055x + 0.079x^2 - 0.002x^3 \quad (1)$$

where x is the distance between the magnet and the hall-effect sensor output voltage in millimeter and y is the corresponding output voltage of hall-effect sensor distance in volt. We can use look-up table or transfer function to quickly find out the gap between the magnet and the hall-effect sensor. Besides, performance of a hall-effect sensor was guaranteed over an extended temperature range from its datasheets. We did not make temperature calibration for the hall-effect sensor prior to starting experiments.

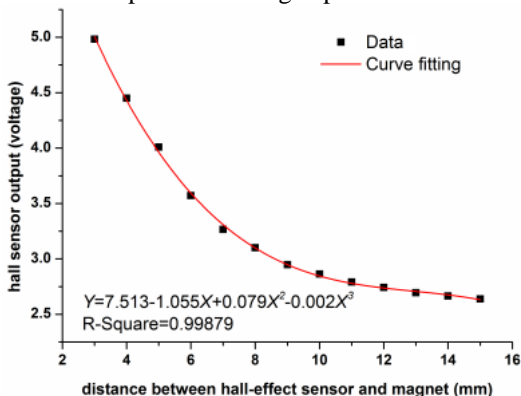


Figure 11: The data and fitting curve of the output voltage of the hall-effect sensor versus distance between hall-effect sensor and magnet.

When the maximum number (1024) of sensor data is reached, the host controller creates a new file to a disk. In order to save disk space, a gzip utility is used for compression of the sensor data. After uncompressed file, the sensor data were shown in Figure 12, each line represents a

data and time stamp, sensor ID, output voltage of a hall-effect sensor and ends with a newline character.

hall-effect sensor			
Date and time stamp	sensor ID	output voltage of sensor	
2014-01-06 16:19:06.969	@ H-2	: 2.72722752888997	
2014-01-06 16:19:07.269	@ H-2	: 2.72717793782552	
2014-01-06 16:19:07.419	@ H-2	: 2.72728665669759	
2014-01-06 16:19:07.439	@ H-2	: 2.72714233398438	
2014-01-06 16:19:07.469	@ H-2	: 2.72726631164551	
2014-01-06 16:19:07.499	@ H-2	: 2.72732543945313	
2014-01-06 16:19:07.529	@ H-2	: 2.72725931803385	
2014-01-06 16:19:07.559	@ H-2	: 2.72722053527832	

Figure 12: Hall-effect sensor record file.

Figure 13 shows the evolution of signals of the hall-effect sensors during the monitoring scour experiment. A cylinder pier model is used for these tests. Some of the hall-effect sensor modules (sensor module 4-10) are completely submerged under sand; the others (sensor module 1-3) are left in the air.

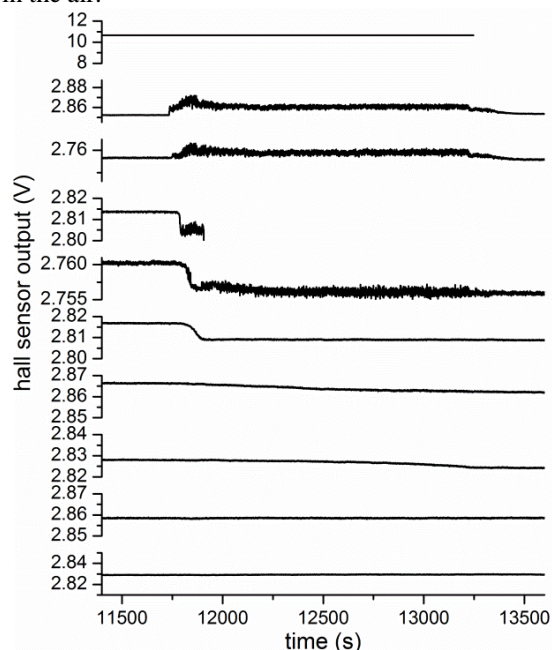


Figure 13: Real-time monitor output voltages of all of hall-effect sensor modules during scour experiment. Plots from top to bottom were corresponded from hall-effect module 1 to 10.

At ca. 10000 s, the inlet valve is ON. At 11733s, water flow starts striking the thin metal strips of the hall-effect sensor module 2 and 3, and their output voltage abruptly grows up due to bending of the thin metal strips caused by the water flow. It is worth knowing that quiver of voltage of the hall-effect sensors were strongly depended on the rate of flow water (data was not shown in here). The output voltages of the hall-effect sensor module 4, 5, and 6 are suddenly dropped down at 11787, 11834, and 11868, respectively. The out voltage of the hell-effect sensor drops so quickly meaning that the sand around the sensor node is totally removed by scour process. However, the rate of change of the output voltage of the hall-effect sensor module 7 and 8 are slower than that of module 4, 5, and 6. It reflects that the scour processes are slow and sand around the hall-effect

sensor module is just partially removed during scour process. The output voltages of the hall-sensor module 9 and 10 almost have no clear drop, so the sand still covers them well. Moreover, the hall-sensor module 1 and 4 are broken due the leaking water from imperfect silicon package sites. Figure 14 shows the pier model before, under, after scour experiment.

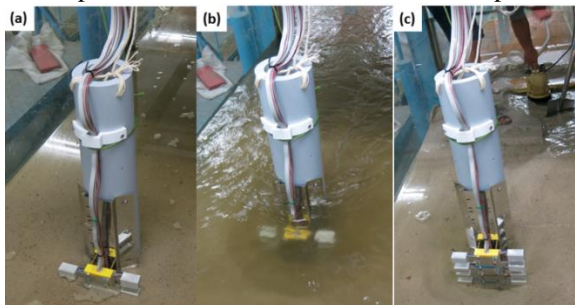


Figure 14: Photos of pier model (a) before, (b) under, and (c) after scour experiment.

In order to sense the scour event more sensitivity by the hall-effect sensor, we try to amplify the change of output voltage of the hall-sensor module after scour event, as shown in Figure 15..

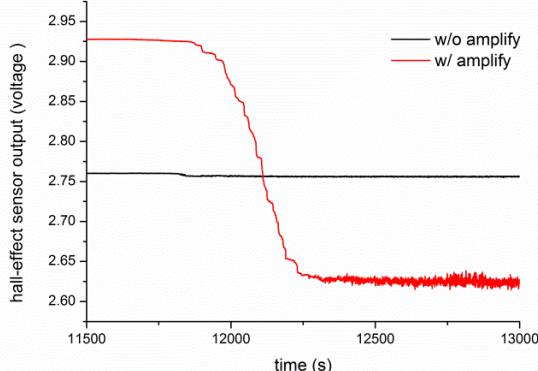


Figure 15: Real-time monitor output voltages of the hall-effect sensor modules with and without amplified signals during scour experiment.

We know that the output voltage of the hell-effect sensor strongly depends on the distance of the magnet and the hall-effect sensor. Therefore, we make the distance between the magnet and the hall-effect sensor get closer during install sensor node. The change of voltage of the hall-effect sensor is enhanced ca. thirty fold that of before original setup, as shown in Figure 15.

IV. CONCLUSION

Comparison of existing system for monitoring bridge scour is shown in Table I. In this study, we have proposed the architecture of real-time bridge pier scouring monitoring system featuring hall-effect sensors. Our proposed real-time monitoring system offers the advantage of low-cost and easy mass deployment. The overall cost for single sensor node of our proposed work is at least 40% less expensive than existing solutions (TDR).

TABLE I. COMPARISON OF EXISTING SYSTEM FOR MONITORING BRIDGE SCOUR

	TDR	Radar	FBG	This work
Cost (\$)	>250	>3500	240 ^a	~100
Resolution (cm)	2.5	10	10	2.5
Temperature effect	Yes	Yes	Yes	NO
work environment	Water; Sand	Air	Water; Sand	Water; Sand
Real-time	Yes	No	Yes	Yes

a. This price is only for sensor.

Our bridge pier scour monitoring system with a solution of 2.5 cm is demonstrated. Furthermore, we also have developed the Bridge Surveillance program with friendly GUI, which automatically collects data of each sensor node. Therefore, it is practical to use our proposed real-time scour monitoring system for diagnosis bridge pier scour events. Next step, we will further widespread implementation in the field.

REFERENCE

- [1] J. C. Chen, C. D. Jan, and W. S. Huang, "Characteristics of Rainfall Triggering of Debris Flows in the Chenyulan Watershed, Taiwan," *Natural Hazards and Earth System Sciences*, vol. 13, 2013, pp. 1015-1023.
- [2] H. Wang, S. C. Hsieh, C. Lin, and C. Y. Wang, "Forensic Diagnosis on Flood-Induced Bridge Failure. I: Determination of the Possible Causes of Failure," *Journal of Performance of Constructed Facilities*, vol. 28, Feb. 2014, pp. 76-84.
- [3] L. J. Prendergast, "A Review of Bridge Scour Monitoring Techniques," *Journal of Rock Mechanics and Geotechnical Engineering* vol. 6, 2014, pp. 138-149.
- [4] J. Y. Lu, J. H. Hong, C. C. Su, C. Y. Wang, and J. S. Lai, "Field Measurements and Simulation of Bridge Scour Depth Variations During Floods," *Journal of Hydraulic Engineering-Asce*, vol. 134, Jun. 2008, pp. 810-821.
- [5] X. B. Yu, and X. Yu, "Laboratory Evaluation of Time-Domain Reflectometry for Bridge Scour Measurement: Comparison with the Ultrasonic Method," *Advances in Civil Engineering*, vol. 2010, 2010, pp. 1-12.
- [6] Y.-B. Lin, J.-S. Lai, K.-C. Chang, W.-Y. Chang, F.-Z. Lee, and Y.-C. Tan, "Using MEMS Sensor in the Bridge Scour Monitoring System," *Journal of the Chinese Institute of Engineers*, vol. 33, Jan, 2010, pp. 25-35.